A Localization Error Upper-bound with Range Measurements to Transmitters with Uncertain Positions

Artun Sel, Samer Hayek, and Zaher M. Kassas
Electrical and Computer Engineering, The Ohio State University, Columbus, OH 43210, USA
Emails: artunsel@ieee.org, watchihayek.1@osu.edu, zkassas@ieee.org

***Abstract*—A localization upper-bound with range measurements to transmitters whose positions are uncertain is derived. The transmitters' positions uncertainty is known to be bounded by a disk with a known radius ε. First, assuming that only one of the transmitters' positions is uncertain (while the rest are perfectly known), an analytic solution is derived for the inaccurate transmitter position within the uncertainty disk, which maximizes the ranging error. This leads to establishing a localization error upper-bound. To demonstrate the applicability of the upper-bound to the case of multiple uncertain transmitter positions, numerical simulations are presented demonstrating that the derived upper-bound still holds. Experimental results are presented of a vehicle navigating in GPS-denied environment, making pseudorange measurements to 7 cellular transmitters, whose positions are uncertain. The experimental results demonstrate the applicability of the upper-bound in predicting the worst-case vehicle localization performance.**

***Index Terms*—Localization, positioning, navigation, error upper-bound, uncertain maps**

I. Introduction

In recent years, various methods have been explored to enhance positioning accuracy, especially in scenarios where the reliability of global navigation satellite systems (GNSS) is compromised [1]–[5]. Relying solely on GNSS for determining essential motion variables is not always feasible due to potential signal loss, degradation, or cyberattacks. A more robust strategy involves leveraging diverse transmitting sources for positioning to ensure redundancy and backup [6], [7].

One promising source that has gained considerable attention is the use of terrestrial signals [8], [9], whether dedicated [10] or non-dedicated (e.g., cellular [11], [12], digital television [13], [14], and FM radio [15], [16]). Here, the receiver produces range-type measurements from received signals (e.g., pseudorange, carrier phase, or Doppler).

An important consideration when using terrestrial sources for localization is knowledge of the transmitters' positions [17]. While radio simultaneous localization and mapping (radio SLAM) offers a relief [18], as the transmitters' positions are continuously refined, receiver localization may not be sufficiently accurate during the initial (transient) stages, especially if the transmitters' uncertainty is large [19]. Even in the case when the transmitters' positions are mapped *a priori* [20], mapping errors on the order of a few meters could exist, raising the following particularly important question for safety-critical systems (e.g., self-driving cars and unmanned aerial systems): given a map of uncertain transmitter positions to which the receiver makes range measurements, what is the upper-bound on receiver localization error?

The recent literature considered the problem of position estimation with uncertain source parameters [21]. In [22] a semi-definite program was derived to deal with non-convexity of source localization from signal time-of-arrival (TOA) measurements with unknown start transmission time and sensor position uncertainties. In [23], source localization based on superimposed received signal strength as a sparse signal recovery problem was proposed to deal with uncertain sensor positions. In [24], cellular signals were used for localization in which multipath component delays were estimated and the localization was formulated as a data association problem. In [25], measurement error was studied for a time-difference-of-arrival (TDOA) problem and a nonlinear constraint was proposed to be imposed on the nonlinear least-squares-based optimization algorithm. In [26], passive localization of a moving source in the presence of random sensor location errors was considered by utilizing TDOA and frequency difference of arrival measurements. In [27], an improved robust TOA-based source localization method was developed in the presence of sensor location uncertainty. In [28], a localization problem was considered using TDOA between the direct and scattered signals, where the position of the scatterer is erroneous. In [29], spatiotemporal uncertainties arising from asynchronous signals and limited, inaccurate source location information was addressed by formulating a clock parameter vector elimination-based semidefinite program. In [30], the localization error sensitivity to transmitter position error was analyzed via a robust estimation formalism.

This paper focuses on the impact of using uncertain transmitter positions for receiver localization. When the transmitter positions are accurately known, standard methods can effectively estimate the receiver's position. However, when the positions are erroneous, it becomes essential to establish a bound on the localization error. This bound is also useful in situations where radio SLAM is adopted. The upper-bound is derived by formulating the problem as a min-max optimization problem [31], [32]. First, assuming that only

This work was supported in part by the National Science Foundation (NSF) under Grant 2240512 and in part by the U.S. Department of Transportation under Grant 69A3552348327 for the CARMEN+ UTC.

one of the transmitters' positions is uncertain (while the rest are perfectly known), an analytic solution is derived for the inaccurate transmitter position within the uncertainty disk, which maximizes the ranging error. This leads to establishing a localization error upper-bound. Due to the mathematical complexity of generalizing the derivation to the case where all transmitters are uncertain, numerical simulations are presented demonstrating that the derived upper-bound holds for the case where all transmitter positions are uncertain. Experimental results are presented of a vehicle navigating in GPS-denied environment, making pseudorange measurements to 7 cellular transmitters, whose positions are uncertain. The experimental results demonstrate the applicability of the upper-bound in predicting the worst-case vehicle localization performance.

This paper is organized as follows. Section II describes the problem. Section III derives the upper-bound. Numerical and experimental results are presented in Sections IV and V, respectively. Concluding remarks are given in Section VI.

II. Problem Description

Consider the problem of localizing a receiver, whose position is denoted by $\boldsymbol{y}$, using range measurements to multiple randomly distributed transmitters. It is assumed that the receiver has an uncertain map of the transmitters' positions, whereby the true transmitter's position, denoted by $\boldsymbol{x_i}$, is within a disk of radius ε, centered around the inaccurate position, denoted $\tilde{\boldsymbol{x}}_{\boldsymbol{i}}$, reported in the map. Using the inaccurate transmitters' positions results in an erroneous receiver estimate, due to the model mismatch between the assumed range and the true range (see Fig. 1). What is the localization error upper-bound due to using the inaccurate tower positions?

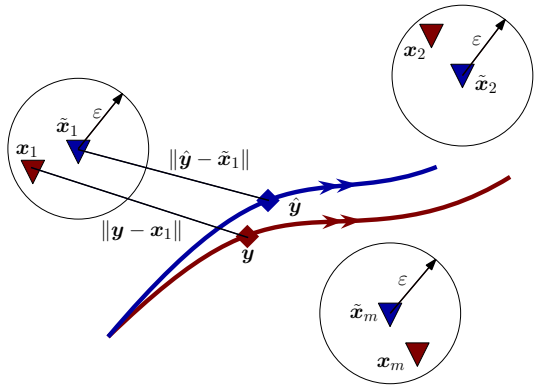

Fig. 1. A receiver localizes itself with range measurements from three transmitters. The receiver has an inaccurate knowledge of the transmitters' positions, denoted $\{\tilde{\boldsymbol{x}}_i\}_{i=1}^3$. The true transmitters' positions, denoted $\{\boldsymbol{x}_i\}_{i=1}^3$, are known to lie within a disk of radius ε. The true and the erroneous estimated receiver trajectories are given in red and blue, respectively.

III. Upper-bound Derivation

For the nominal case, whereby the transmitters' positions are accurately known, the localization problem is stated as

$$\hat{\boldsymbol{y}} = \underset{\hat{\boldsymbol{y}}}{\operatorname{argmin}} \sum_{i=1}^{M} \left[\|\boldsymbol{x}_i - \boldsymbol{y}\| - \|\boldsymbol{x}_i - \hat{\boldsymbol{y}}\| \right]^2, \tag{1}$$

where $\boldsymbol{y} \in \mathbb{R}^2$ denotes the true receiver position, $\hat{\boldsymbol{y}} \in \mathbb{R}^2$ denotes the receiver's position estimate, and $\boldsymbol{x}_i \in \mathbb{R}^2$ represents the position of the i^{th} transmitter.

Now, consider the case where the transmitters' positions are erroneous, denoted by $\tilde{\boldsymbol{x}}_i \in \mathbb{R}^2$, and assume that the error in their positions is within an uncertainty set, defined by

$$\boldsymbol{\mathcal{S}_i} = \{\tilde{\boldsymbol{x}}_{\boldsymbol{i}} : \|\tilde{\boldsymbol{x}}_{\boldsymbol{i}} - \boldsymbol{x_i}\| \leq \varepsilon_1\}, \quad \forall i = 1, \ldots, M. \tag{2}$$

In what follows, an upper-bound will be derived on the localization error induced by using inaccurate transmitter positions. This problem can be cast as

$$\max_{\tilde{\boldsymbol{x}}_{\boldsymbol{i}} \in \boldsymbol{\mathcal{S}_i}} \|\boldsymbol{y} - [\underset{\hat{\boldsymbol{y}}}{\operatorname{argmin}} \sum_{i=1}^{M} (\|\boldsymbol{x_i} - \boldsymbol{y}\| - \|\tilde{\boldsymbol{x}}_{\boldsymbol{i}} - \hat{\boldsymbol{y}}\|)^2]\|. \tag{3}$$

Using (2), (3) can be expressed as

$$\max_{\|\boldsymbol{\xi_i}\| \leq \varepsilon_1} \|\boldsymbol{y} - [\underset{\hat{\boldsymbol{y}}}{\operatorname{argmin}} \sum_{i=1}^{M} (\|\boldsymbol{x_i} - \boldsymbol{y}\| - \|(\boldsymbol{x_i} + \boldsymbol{\xi_i}) - \hat{\boldsymbol{y}}\|)^2]\|, \tag{4}$$

where $\boldsymbol{\xi_i} \in \mathbb{R}^2$ represents the error in the i^{th} tower position that induces the estimation error. It is worth noting that neither the maximization nor the minimization part has a readily available structure that can be directly exploited like convexity or concavity, but the following subproblem is useful to reveal some structure. First, by constraining the error terms to only one term (i.e., only one of the transmitters has an inaccurate position), then by considering the problem of finding the maximum error, the main problem can be expressed as the following bilevel optimization problem

$$\max_{\|\boldsymbol{\xi_i}\| \leq \varepsilon_1} \|\boldsymbol{y} - \hat{\boldsymbol{y}}_{\boldsymbol{\xi_1}}\|, \tag{5}$$

where $\hat{\boldsymbol{y}}_{\boldsymbol{\xi_1}}$ is explicitly given by

$$\hat{\boldsymbol{y}}_{\boldsymbol{\xi_1}} = \left\{ \begin{array}{ll} \underset{\hat{\boldsymbol{y}}}{\operatorname{argmin}} & \sum_{i=1}^{M} [r_i - r_{\xi_{1i}}]^2 \\ \text{s.t.} & r_i = \|\boldsymbol{x_i} - \boldsymbol{y}\| \\ & r_{\xi_{1i}} = \|(\boldsymbol{x_i} + \boldsymbol{\xi_1}\delta_{1i}) - \hat{\boldsymbol{y}}\| \end{array} \right\}, \tag{6}$$

where instead of $\{\boldsymbol{\xi_i}\}_{i=1}^M$, only the error for the first transmitter is considered. The term δ_{1i} takes the value 1 for $i = 1$ and 0 otherwise. Note that the term $\hat{\boldsymbol{y}}_{\boldsymbol{\xi_1}}$ is a function of $\boldsymbol{\xi_1}$ for a given $\boldsymbol{x_i}$ and $\boldsymbol{y}$, i.e., how the error affects the estimation depends on the geometry of the problem. In an environment containing 2 or more transmitters, where only the first transmitter's position is erroneous, it is reasonable to expect the error-maximizing error term to be on the line that contains $\boldsymbol{x_1}$ and $\boldsymbol{y}$, since that would correspond to the error term that maximizes the predicted range error. This line will be denoted LoS-line (line-of-sight), and it extends to infinity in both directions. However, that error is not the exact solution to the problem since the given two optimization problems are not equivalent to each other, namely

$$\begin{aligned} &\underset{\|\boldsymbol{\xi_1}\| \leq \varepsilon_1}{\operatorname{argmax}} \left\| \boldsymbol{y} - \left[\underset{\hat{\boldsymbol{y}}}{\operatorname{argmin}} \sum_{i=1}^{M} (r_i - r_{\xi_{1i}})^2 \right] \right\| \\ &\neq \underset{\|\boldsymbol{\xi_1}\| \leq \varepsilon_1}{\operatorname{argmax}} \sum_{i=1}^{M} (r_i - r_{\xi_{1i}})^2, \end{aligned} \tag{7}$$

which is due to $\hat{\boldsymbol{y}}_{\boldsymbol{\xi_1}}$ being a function of the error, which is neglected by the latter optimization problem.

Nevertheless, numerical simulations suggested that although the exact solution may not lie on the LoS-line, it would be a good initial point for a search algorithm, as often the optimal error is close to one of the two points given by the LoS-line intersecting the boundary of the uncertainty set, parameterized by ε_1. That leads to the question: under what condition is the estimation error-maximizing error term on the LoS-line or sufficiently close?

Theorem 1. *The solution to the optimization problem*

$$\max_{\|\boldsymbol{\xi_1}\|\leq\varepsilon_1} \|\boldsymbol{y} - [\operatorname*{argmin}_{\hat{\boldsymbol{y}}} \sum_{i=1}^{M} (\|\boldsymbol{x_i}-\boldsymbol{y}\| - \|(\boldsymbol{x_i}+\boldsymbol{\xi_1}\delta_{1i}) - \hat{\boldsymbol{y}}\|)^2]\|,$$

denoted $\boldsymbol{\xi_1^*}$*, satisfies*

$$\lim_{\left(\frac{R_{\min}}{\varepsilon_1}\right)\to\infty} \min_{j\in\{1,2\}} \left\{\|\boldsymbol{\xi_1^*} - \boldsymbol{a_j}\|\right\} = 0,$$

where $R_{\min}$ *is defined by*

$$R_{\min} = \min_{i\in\{1,\dots,M\}} \{\|\boldsymbol{x_i} - \boldsymbol{y}\|\},$$

and $\{\boldsymbol{a_1}, \boldsymbol{a_2}\}$ *denote the points defined by*

$$\boldsymbol{a_1} = \varepsilon_1 \frac{(\boldsymbol{y}-\boldsymbol{x_1})}{\|\boldsymbol{y}-\boldsymbol{x_1}\|}, \boldsymbol{a_2} = -\varepsilon_1 \frac{(\boldsymbol{y}-\boldsymbol{x_1})}{\|\boldsymbol{y}-\boldsymbol{x_1}\|}$$

Proof. The optimization problem

$$\operatorname*{argmin}_{\hat{\boldsymbol{y}}} \sum_{i=1}^{M} \left(\|\boldsymbol{x_i}-\boldsymbol{y}\| - \|\boldsymbol{x_i}+\boldsymbol{\xi_1}\delta_{1i} - \hat{\boldsymbol{y}}\|\right)^2$$

can be solved by nonlinear least-squares, for a given initial estimate that is sufficiently close to $\boldsymbol{y}$, as

$$\hat{\boldsymbol{y}}(\boldsymbol{\xi_1})^{(k+1)} = \hat{\boldsymbol{y}}^{(k)} + \boldsymbol{\mathcal{H}}_{\boldsymbol{\xi_1}} \tilde{\boldsymbol{r}}_{\boldsymbol{\xi_1}}(\hat{\boldsymbol{y}}^{(k)})$$
$$\hat{\boldsymbol{y}}^{(k+1)} = \hat{\boldsymbol{y}}^{(k)} + \boldsymbol{\mathcal{H}} \tilde{\boldsymbol{r}}(\hat{\boldsymbol{y}}^{(k)})$$

$$\boldsymbol{\mathcal{H}}_{\boldsymbol{\xi_1}} = \left[\left(\mathbf{H}_\xi{}^\mathsf{T}\mathbf{H}_\xi\right)^{-1}\mathbf{H}_\xi{}^\mathsf{T}\right], \quad \boldsymbol{\mathcal{H}} = \left[\left(\mathbf{H}^\mathsf{T}\mathbf{H}\right)^{-1}\mathbf{H}^\mathsf{T}\right],$$

where $\boldsymbol{\mathcal{H}}_{\boldsymbol{\xi_1}}$ and $\boldsymbol{\mathcal{H}}$ correspond to the perturbed and the nominal cases, respectively. The residual terms are given by

$$\tilde{\boldsymbol{r}}_{\boldsymbol{\xi_1}}(\hat{\boldsymbol{y}}^{(k)}) = \begin{bmatrix} \|\boldsymbol{x_1}-\boldsymbol{y}\| - \|(\boldsymbol{x_1}+\xi_1) - \hat{\boldsymbol{y}}^{(k)}\| \\ \vdots \\ \|\boldsymbol{x_M}-\boldsymbol{y}\| - \|\boldsymbol{x_M} - \hat{\boldsymbol{y}}^{(k)}\| \end{bmatrix}$$

$$\tilde{\boldsymbol{r}}(\hat{\boldsymbol{y}}^{(k)}) = \begin{bmatrix} \|\boldsymbol{x_1}-\boldsymbol{y}\| - \|\boldsymbol{x_1} - \hat{\boldsymbol{y}}^{(k)}\| \\ \vdots \\ \|\boldsymbol{x_M}-\boldsymbol{y}\| - \|\boldsymbol{x_M} - \hat{\boldsymbol{y}}^{(k)}\| \end{bmatrix},$$

where $\hat{\boldsymbol{y}}^{(k)}$ denotes the current estimate at the iteration step k and $\mathbf{H}$ denotes the Jacobian of the cost function with respect to the decision variable $\hat{\boldsymbol{y}}$ for the case where the error term is constrained to be equal to zero. The $\mathbf{H}_{\xi_1}$ term represents the same parameter without zero magnitude constraint on the error; therefore, this quantity is a function of $\boldsymbol{\xi_1}$. The terms $\hat{\boldsymbol{y}}^{(k+1)}$ and $\hat{\boldsymbol{y}}(\boldsymbol{\xi_1})^{(k+1)}$ denote the next estimates of the position for the nominal and perturbed problems, respectively. For both of the problems, if the same estimates $\hat{\boldsymbol{y}}^{(k)}$ are used, in the next iteration, the error is given by

$$\left\|\hat{\boldsymbol{y}}(\boldsymbol{\xi_1})^{(k+1)} - \hat{\boldsymbol{y}}^{(k+1)}\right\| = \left\|\boldsymbol{\mathcal{H}}_{\xi_1}\tilde{\boldsymbol{r}}_{\boldsymbol{\xi_1}}(\hat{\mathbf{y}}^{(k)}) - \boldsymbol{\mathcal{H}}\tilde{\boldsymbol{r}}(\hat{\boldsymbol{y}}^{(k)})\right\|.$$

As shown in Appendix A, the following can be stated

$$\lim_{\left(\frac{R_{\min}}{\varepsilon_1}\right)\to\infty} \|\boldsymbol{\mathcal{H}}_{\xi_1} - \boldsymbol{\mathcal{H}}\| = 0. \tag{8}$$

Although the limit in (8) means that the transmitter is located infinitely away from the receiver, which is unrealistic, numerical simulations suggested that for transmitters that are sufficiently faraway, $\|\boldsymbol{\mathcal{H}}_{\xi_1} - \boldsymbol{\mathcal{H}}\|$ is negligible compared to $\|\boldsymbol{\mathcal{H}}\|$. As such, the following simplification can be made

$$\left\|\hat{\boldsymbol{y}}(\boldsymbol{\xi_1})^{(k+1)} - \hat{\boldsymbol{y}}^{(k+1)}\right\| = \left\|\boldsymbol{\mathcal{H}}\left\{\tilde{\boldsymbol{r}}_{\boldsymbol{\xi_1}}(\hat{\boldsymbol{y}}^{(k)}) - \tilde{\boldsymbol{r}}(\hat{\boldsymbol{y}}^{(k)})\right\}\right\|.$$

By the Cauchy-Schwarz inequality

$$\left\|\hat{\boldsymbol{y}}(\boldsymbol{\xi_1})^{(k+1)} - \hat{\boldsymbol{y}}^{(k+1)}\right\| \leq \|\boldsymbol{\mathcal{H}}\| \left\|\tilde{\boldsymbol{r}}_{\boldsymbol{\xi_1}}(\hat{\boldsymbol{y}}^{(k)}) - \tilde{\boldsymbol{r}}(\hat{\boldsymbol{y}}^{(k)})\right\|,$$

which leads to an upper-bound on the norm of the error term, leading to the following problem

$$\operatorname*{argmax}_{\|\boldsymbol{\xi_1}\|\leq\varepsilon_1} \left\|\hat{\boldsymbol{y}}(\boldsymbol{\xi_1})^{(k+1)} - \hat{\boldsymbol{y}}^{(k+1)}\right\|. \tag{9}$$

By using $\boldsymbol{y}$ as the initial estimate, (9) can be approximated by

$$\operatorname*{argmax}_{\|\boldsymbol{\xi_1}\|\leq\varepsilon_1} \left\| \begin{matrix} \|\boldsymbol{x_1}-\boldsymbol{y}\| - \|(\boldsymbol{x_1}+\boldsymbol{\xi_1})-\boldsymbol{y}\| \\ \vdots \\ \|\boldsymbol{x_M}-\boldsymbol{y}\| - \|\boldsymbol{x_M}-\boldsymbol{y}\| \end{matrix} \right\|,$$

which amounts to finding the error term that maximizes the norm of the difference between the true and estimated range. Using the structure of the problem, the following equivalent problem can be written

$$\operatorname*{argmax}_{\|\boldsymbol{\xi_1}\|\leq\varepsilon_1} \left|\|\boldsymbol{x_1}-\boldsymbol{y}\| - \|(\boldsymbol{x_1}+\boldsymbol{\xi_1})-\boldsymbol{y}\|\right|.$$

Arranging the terms and approximating the second expression by its Taylor approximation around the nominal case, yields

$$\|[\boldsymbol{x_1}-\boldsymbol{y}]+\boldsymbol{\xi_1}\| \approx \|\boldsymbol{x_1}-\boldsymbol{y}\| + [\boldsymbol{\xi_1}]^\mathsf{T}\frac{\boldsymbol{x_1}-\boldsymbol{y}}{\|\boldsymbol{x_1}-\boldsymbol{y}\|}.$$

The problem can be simplified to

$$\operatorname*{argmax}_{\|\boldsymbol{\xi_1}\|\leq\varepsilon_1} \left| \left[\boldsymbol{\xi}_1^\mathsf{T}\frac{\boldsymbol{x_1}-\boldsymbol{y}}{\|\boldsymbol{x_1}-\boldsymbol{y}\|}\right] \right| \in \left\{\pm\varepsilon_1\frac{\boldsymbol{x_1}-\boldsymbol{y}}{\|\boldsymbol{x_1}-\boldsymbol{y}\|}\right\}.$$

□

Theorem 1 essentially states that the maximizer error is on the intersection between the LoS-line and the boundary of the uncertainty set. The generalization of this theorem to the case where all transmitters have an inaccurate position is mathematically involved. The next section will demonstrate via numerical simulations that the upper-bound derived via Theorem 1 to multiple transmitters essentially holds. The mathematical proof; however, is deferred for future work.

For the case where multiple transmitters are sufficiently faraway from the receiver, the utility of Theorem 1 is that the error-maximizer error term can be computed by exhaustively searching from the set

$$S_\xi := \left\{ \begin{pmatrix} \boldsymbol{\xi_1} \\ \vdots \\ \boldsymbol{\xi_M} \end{pmatrix} \in \mathbb{R}^{2M} \,\middle|\, \boldsymbol{\xi_i} = \pm\varepsilon \frac{\boldsymbol{x_i} - \boldsymbol{y}}{\|\boldsymbol{x_i} - \boldsymbol{y}\|} \right\}. \quad (10)$$

Algorithm 1 outlines the upper-bound computation steps.

Algorithm 1 Upper-bound computation

1: Initialization: For a given receiver trajectory $\{\boldsymbol{y}(k)\}_{k=1}^{N}$, transmitter positions $\{\boldsymbol{x_i}\}_{i=1}^{M}$, and uncertainty disk radius ε_1

2: **for** $k = 1, \ldots, N$ **do**

3: Generate all possible $\{\boldsymbol{x_i}'\}_j$ terms s.t.

$$\|\boldsymbol{x_i} - \boldsymbol{x_i}'\| \in \{\|\boldsymbol{x_i} - \boldsymbol{x_i}'\| \leq \varepsilon_1 | \|\boldsymbol{x_i} - \boldsymbol{y}(k)\| \pm \varepsilon_1\}$$
$$\forall i = 1, \ldots, M, \;\; \forall j = 1, \ldots, 2^M$$

4: **for** $j = 1, \ldots, 2^M$ **do**

5: Compute $\hat{\boldsymbol{y}}$ from

$$\hat{\boldsymbol{y}}_j = \arg\min_{\hat{\boldsymbol{y}}} \sum_{i=1}^{M} \left[\|\boldsymbol{x_i} - \boldsymbol{y}(k)\| - \|\boldsymbol{x_i}' - \hat{\boldsymbol{y}}\| \right]^2$$

6: **end for**

7: Find $\{\boldsymbol{x_i}'\}_j^*$ s.t.

$$j = \arg \max_{j=1,\ldots,2^M} \left\| \boldsymbol{y}(k) - \hat{\boldsymbol{y}}_j \right\|$$

8: **end for**

IV. Numerical Simulations

This section presents numerical simulations demonstrating the upper-bound computed via Algorithm 1 to solve the optimization problem in (3). The simulations considered a receiver moving along a trajectory in an environment comprising 3 transmitters as shown in Fig. 2. For each transmitter, a grid of erroneous transmitter positions was generated within an uncertainty disk with radius $\varepsilon = 20$, centered around the true transmitter position.

To demonstrate that the computed localization error upper-bound holds, the following was performed. First, at each time step along the receiver's trajectory, the position of the receiver was estimated using erroneous transmitter positions from the generated grid of inaccurate transmitter positions. The resulting localization error is shown as the blue point cloud in Fig. 3. Next, the position of the receiver was estimated by first, computing the error-maximizing erroneous transmitter positions as described by Algorithm 1, and then using that inaccurate transmitter to estimate the receiver's position. The resulting localization error is shown in red in Fig. 3, which demonstrates that the upper-bound is valid for exhaustively sampled erroneous transmitter position within the uncertainty region.

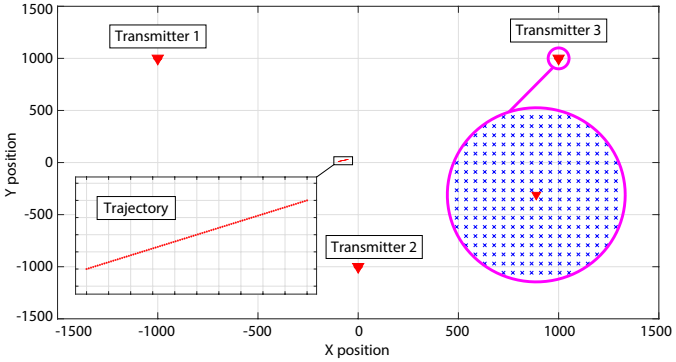

Fig. 2. Simulated environment showing the receiver trajectory, transmitter positions, and grid of erroneous transmitter positions within the uncertainty region (indicated by blue-crosses).

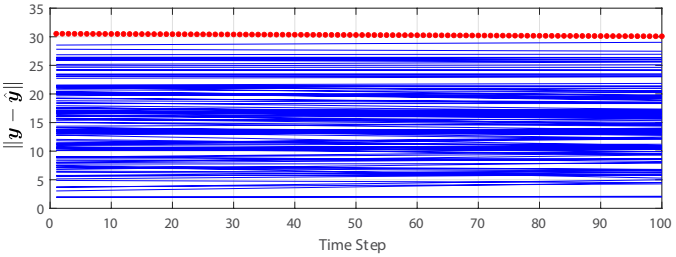

Fig. 3. Localization error along the receiver's trajectory for (1) exhaustively sampled erroneous transmitter positions (blue) and (2) upper-bound (red).

V. Experimental Results

This section presents experimental results demonstrating the utility of the upper-bound for a vehicle navigating in a GPS-denied environment with pseudorange measurements from 7 cellular transmitters with inaccurately known positions.

A. Experimental Setting

A vehicle was driven in a GPS-denied environment at Edwards Air Force Base, California, USA during live GPS jamming. The vehicle was equipped with a software-defined radio (SDR) capable of producing psuedorange measurements to cellular transmitters in the environment. The experimental setup and relevant models are described in [33], [34]. Since the developed upper-bound assumed range measurements, while the SDR produced pseudorange measurements, the pseudoranges were converted to range measurements as follows. A Kalman Filter was implemented using the vehicle's true trajectory and the true transmitter positions to estimate the clock errors along the vehicle's trajectory. The estimated clock errors were then subtracted from the pseudoranges.

B. Experimental Results

To demonstrate the upper-bound, two cases were considered:

1) **Estimation with inaccurate transmitter positions**: First, for each transmitter, 300 erroneous positions were uniformly sampled from an uncertainty disk, centered around the true transmitter position with a radius of $\varepsilon = 20$ m. The receiver's position was estimated using the range measurements in (1). The resulting localization error is plotted as the point cloud in blue in Fig. 4.

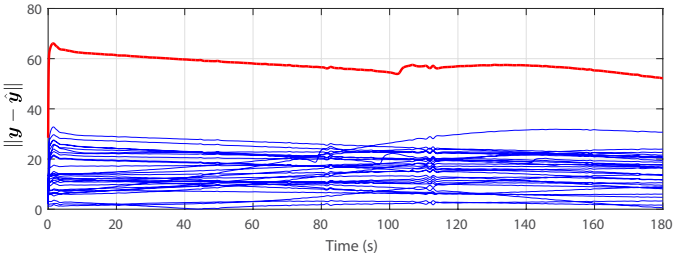

Fig. 4. Experimental localization error along the vehcile's trajectory for (1) sampled erroneous transmitter positions (blue) and (2) upper-bound (red).

2) **Estimation with an error-maximizing inaccurate transmitter position**: At each time-step, using Algorithm 1, the error-maximizing erroneous transmitter positions were computed. Next, the receiver's position was estimated using range measurements by solving the optimization problem, resulting in the localization error upper-bound. The resulting upper-bound is plotted in red in Fig. 4. It can be seen that the upper-bound holds throughout the trajectory. It is worth noting that the upper bound is looser than the simulation results in Section IV, since in the simulations, the samples were generated finely, while here, due to the heavy computational burden to exhaustively sample the uncertainty region, a smaller number of samples were generated.

Fig. 5 shows the vehicle-mounted receiver's true trajectory, estimated trajectories using the inaccurate sampled transmitter positions, and the estimated trajectories with the error-maximizing erroneous transmitter positions.

VI. Conclusion

Thus paper derived a localization error upper-bound for a receiver utilizing range measurements to uncertain transmitter positions. The derivation assumed the inaccuracy to correspond to a single transmitter (other transmitter positions are known), leading to identifying the inaccurate tower positions yielding the largest localization error, from which the upper-bound is established. To demonstrate the applicability of the upper-bound to the case of multiple uncertain transmitter positions, numerical simulations are presented demonstrating that the derived upper-bound still holds. Experimental results were presented of a vehicle navigating in GPS-denied environment, making pseudorange measurements to 7 cellular transmitters, from which range measurements were computed. The experimental results demonstrated the applicability of the upper-bound in predicting the worst-case localization performance.

Appendix A
Proof of (8)

Proof. The following

$$\lim_{\left(\frac{R_{\min}}{\varepsilon_1}\right)\to\infty} \|\boldsymbol{\mathcal{H}}_{\boldsymbol{\xi}} - \boldsymbol{\mathcal{H}}\| = 0, \tag{11}$$

implies that the matrices get closer to each other in any defined norm as the minimum distance term between the transmitter and the receiver increases. Without loss of generality, consider a planar environment in which the receiver is at the origin and

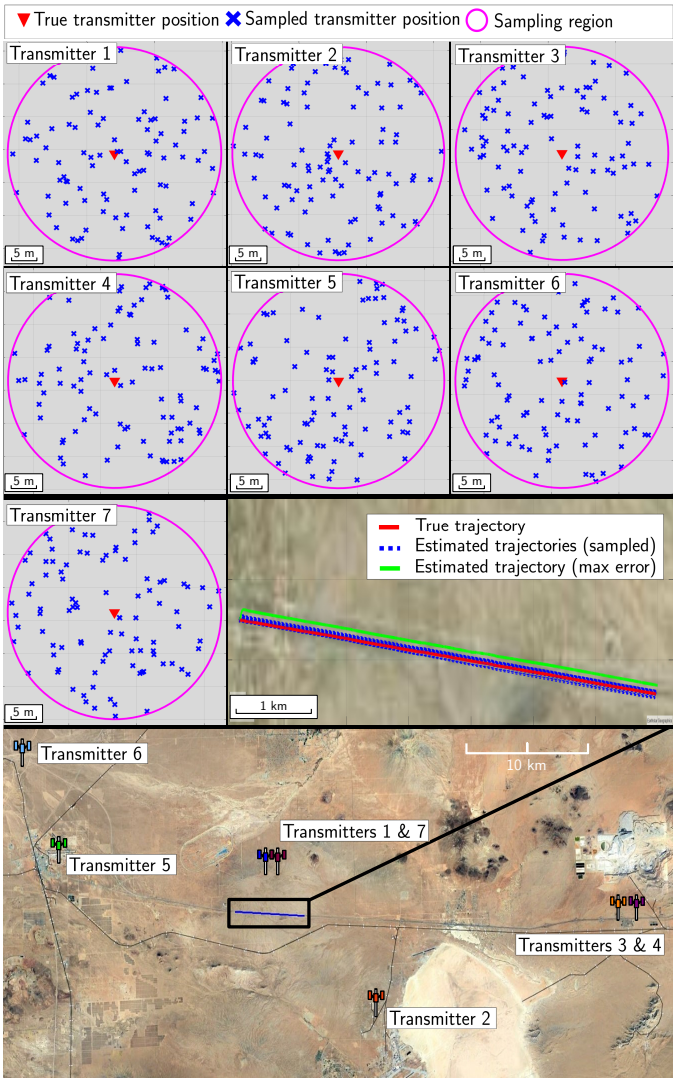

Fig. 5. Experimental results: (i) true transmitters' positions (shown as red triangles), (ii) uncertainty disk and samples of the inaccurate transmitter positions for each transmitter (50 of the 300 samples are shown for ease of visualization), and (iii) vehicle's true trajectory, estimated trajectory due to sampled inaccurate transmitter positions, and estimated trajectory due to error-maximizing erroneous transmitter positions.

the transmitters are randomly distributed around the receiver. Denote the distance between i^{th} transmitter and the receiver by R_i, while α_i represents the corresponding angle. Now, assume that the map of transmitter positions is erroneous and that for all transmitters, the distance between the erroneous position and the true one is ε_1. Denote the angle between the true tower location and the erroneous one by θ_i. Therefore, $\mathbf{H}_\xi$ can be expressed as

$$\mathbf{H}_\xi = \begin{bmatrix} \frac{[x_{11}+\varepsilon_1 \mathtt{C}_{\theta_1}]-y_1}{\left\|\begin{bmatrix} x_{11}+\varepsilon_1\mathtt{C}_{\theta_1} \\ x_{12}+\varepsilon_1\mathtt{S}_{\theta_1}\end{bmatrix}-\boldsymbol{y}\right\|} & \frac{[x_{22}+\varepsilon_1 \mathtt{S}_{\theta_1}]-y_2}{\left\|\begin{bmatrix} x_{21}+\varepsilon_1\mathtt{C}_{\theta_1} \\ x_{22}+\varepsilon_1\mathtt{S}_{\theta_1}\end{bmatrix}-\boldsymbol{y}\right\|} \\ \vdots & \vdots \\ \frac{[x_{M1}+\varepsilon_1 \mathtt{C}_{\theta_M}]-y_1}{\left\|\begin{bmatrix} x_{M1}+\varepsilon_1\mathtt{C}_{\theta_M} \\ x_{M2}+\varepsilon_1\mathtt{S}_{\theta_M}\end{bmatrix}-\boldsymbol{y}\right\|} & \frac{[x_{M2}+\varepsilon_1 \mathtt{S}_{\theta_M}]-y_2}{\left\|\begin{bmatrix} x_{M1}+\varepsilon_1\mathtt{C}_{\theta_M} \\ x_{M2}+\varepsilon_1\mathtt{S}_{\theta_M}\end{bmatrix}-\boldsymbol{y}\right\|} \end{bmatrix}, \tag{12}$$

where $\mathtt{c}_{\theta_i}$ and $\mathtt{s}_{\theta_i}$ denote $\cos(\theta_i)$ and $\sin(\theta_i)$, respectively. To analyze the relationship between $R_{\min}$ and the error between $\boldsymbol{\mathcal{H}}_{\boldsymbol{\xi}}$ and $\boldsymbol{\mathcal{H}}$, R_i is replaced by βR_i, where $\beta \geq 1$. The corresponding $\mathbf{H}_{\xi}$ can be expressed as

$$\mathbf{H}_{\xi} = \begin{bmatrix} \frac{[\beta R_1 \mathtt{c}_{\alpha_1} + \varepsilon_1 \mathtt{c}_{\theta_1}]}{\left\| \begin{bmatrix} \beta R_1 \mathtt{c}_{\alpha_1} + \varepsilon_1 \mathtt{c}_{\theta_1} \\ \beta R_1 \mathtt{s}_{\alpha_1} + \varepsilon_1 \mathtt{s}_{\theta_1} \end{bmatrix} \right\|} & \frac{[\beta R_1 \mathtt{s}_{\alpha_1} + \varepsilon_1 \mathtt{s}_{\theta_1}]}{\left\| \begin{bmatrix} \beta R_1 \mathtt{c}_{\alpha_1} + \varepsilon_1 c_{\theta_1} \\ \beta R_1 \mathtt{s}_{\alpha_1} + \varepsilon_1 s_{\theta_1} \end{bmatrix} \right\|} \\ \vdots & \vdots \\ \frac{[\beta R_M \mathtt{c}_{\alpha_M} + \varepsilon_1 \mathtt{c}_{\theta_M}]}{\left\| \begin{bmatrix} \beta R_M \mathtt{c}_{\alpha_M} + \varepsilon_1 \mathtt{c}_{\theta_M} \\ \beta R_M \mathtt{s}_{\alpha_M} + \varepsilon_1 \mathtt{s}_{\theta_M} \end{bmatrix} \right\|} & \frac{[\beta R_M \mathtt{s}_{\alpha_M} + \varepsilon_1 \mathtt{s}_{\theta_M}]}{\left\| \begin{bmatrix} \beta R_M \mathtt{c}_{\alpha_M} + \varepsilon_1 \mathtt{c}_{\theta_M} \\ \beta R_M \mathtt{s}_{\alpha_M} + \varepsilon_1 \mathtt{s}_{\theta_M} \end{bmatrix} \right\|} \end{bmatrix}. \tag{13}$$

Using (13), it can be shown that

$$\lim_{\beta \to \infty} \|\mathbf{H}_{\xi} - \mathbf{H}\| = 0,$$

which can be written for a general setting as

$$\lim_{\left(\frac{R_{\min}}{\varepsilon_1}\right) \to \infty} \|\boldsymbol{\mathcal{H}}_{\boldsymbol{\xi}} - \boldsymbol{\mathcal{H}}\| = 0.$$

□

REFERENCES

[1] H. Dureppagari, C. Saha, H. Dhillon, and R. Buehrer, "NTN-based 6G localization: Vision, role of LEOs, and open problems," *IEEE Wireless Communications*, vol. 30, no. 6, pp. 44–51, 2023.

[2] T. Janssen, A. Koppert, R. Berkvens, and M. Weyn, "A survey on IoT positioning leveraging LPWAN, GNSS and LEO-PNT," *IEEE Internet of Things Journal*, vol. 10, no. 13, pp. 11135–11159, 2023.

[3] H. Sallouha, S. Saleh, S. De Bast, Z. Cui, S. Pollin, and H. Wymeersch, "On the ground and in the sky: A tutorial on radio localization in ground-air-space networks," *IEEE Communications Surveys & Tutorials*, pp. 1–41, 2024. accepted.

[4] W. Stock, R. Schwarz, C. Hofmann, and A. Knopp, "Survey on opportunistic PNT with signals from LEO communication satellites," *IEEE Communications Surveys & Tutorials*, pp. 1–31, 2024. accepted.

[5] Z. Kassas, S. Kozhaya, H. Kanj, J. Saroufim, S. Hayek, M. Neinavaie, N. Khairallah, and J. Khalife, "Navigation with multi-constellation LEO satellite signals of opportunity: Starlink, Oneweb, Orbcomm, and Iridium," in *Proceedings of IEEE/ION Position, Location, and Navigation Symposium*, pp. 338–343, April 2023.

[6] N. Souli, P. Kolios, and G. Ellinas, "Online relative positioning of autonomous vehicles using signals of opportunity," *IEEE Transactions on Intelligent Vehicles*, vol. 7, no. 4, pp. 873–885, 2022.

[7] M. Jia, J. Khalife, and Z. Kassas, "Performance analysis of opportunistic ARAIM for navigation with GNSS signals fused with terrestrial signals of opportunity," *IEEE Transactions on Intelligent Transportation Systems*, vol. 24, no. 10, pp. 10587–10602, 2023.

[8] Z. Kassas, M. Maaref, J. Morales, J. Khalife, and K. Shamaei, "Robust vehicular localization and map matching in urban environments through IMU, GNSS, and cellular signals," *IEEE Intelligent Transportation Systems Magazine*, vol. 12, pp. 36–52, June 2020.

[9] J. Khalife and Z. Kassas, "Differential framework for submeter-accurate vehicular navigation with cellular signals," *IEEE Transactions on Intelligent Vehicles*, vol. 8, pp. 732–744, January 2023.

[10] J. del Peral-Rosado, A. Yildirim, S. Schlotzer, P. Nolle, S. Razavi, S. Parsawa, R. Mundlamuri, F. Kaltenberger, N. Sirola, S. Garlaschi, L. Canzian, J. Talvitie, I. Lapin, and D. Flachs, "First field trial results of hybrid positioning with dedicated 5G terrestrial and UAV-based non-terrestrial networks," in *Proceedings of ION GNSS Conference*, pp. 1598–1605, September 2023.

[11] J. Tian, L. Fangchi, T. Yafei, and L. Dongmei, "Utilization of non-coherent accumulation for LTE TOA estimation in weak LOS signal environments," *EURASIP Journal on Wireless Communications and Networking*, vol. 2023, no. 1, pp. 1–31, 2023.

[12] A. Winter, A. Morrison, and N. Sokolova, "Analysis of 5G and LTE signals for opportunistic navigation and time holdover," *Sensors*, vol. 24, no. 1, pp. 1–14, 2023.

[13] T. Hong, J. Sun, T. Jin, Y. Yi, and J. Qu, "Hybrid positioning with DTMB and LTE signals," in *Proceedings of International Wireless Communications and Mobile Computing*, pp. 303–307, July 2021.

[14] Z. Jiao, L. Chen, X. Lu, Z. Liu, X. Zhou, Y. Zhuang, and G. Guo, "Carrier phase ranging with DTMB signals for urban pedestrian localization and GNSS aiding," *Remote Sensing*, vol. 15, no. 2, pp. 423–446, 2023.

[15] X. Chen, Q. Wei, F. Wang, Z. Jun, S. Wu, and A. Men, "Super-resolution time of arrival estimation for a symbiotic FM radio data system," *IEEE Transactions on Broadcasting*, vol. 66, pp. 847–856, December 2020.

[16] S. Zheng, J. Hu, L. Zhang, K. Qiu, J. Chen, P. Qi, Z. Zhao, and X. Yang, "FM-based positioning via deep learning," *IEEE Journal on Selected Areas in Communications*, vol. 42, pp. 2568–2584, September 2024.

[17] M. Hameed, M. Philips-Blum, M. Arizabaleta-Diez, and T. Pany, "LTE transmitter states estimation using a combined code and carrier phase observation model," in *Proceedings of IEEE/ION Position, Location, and Navigation Symposium*, pp. 1107–1117, April 2023.

[18] J. Morales and Z. Kassas, "Tightly-coupled inertial navigation system with signals of opportunity aiding," *IEEE Transactions on Aerospace and Electronic Systems*, vol. 57, no. 3, pp. 1930–1948, 2021.

[19] Z. Kassas, N. Khairallah, J. Khalife, C. Lee, J. Jurado, S. Wachtel, J. Duede, Z. Hoeffner, T. Hulsey, R. Quirarte, and R. Tay, "Aircraft navigation in GNSS-denied environments via radio SLAM with terrestrial signals of opportunity," *IEEE Transactions on Intelligent Transportation Systems*, pp. 1–19, 2024. accepted.

[20] J. Morales and Z. Kassas, "Optimal collaborative mapping of terrestrial transmitters: receiver placement and performance characterization," *IEEE Transactions on Aerospace and Electronic Systems*, vol. 54, pp. 992–1007, April 2018.

[21] F. Qiu and W. Zhang, "Position error vs. signal measurements: An analysis towards lower error bound in sensor network," *Digital Signal Processing*, vol. 129, pp. 1–18, September 2022.

[22] Y. Zou and Q. Wan, "Asynchronous time-of-arrival-based source localization with sensor position uncertainties," *IEEE Communications Letters*, vol. 20, pp. 1860–1863, February 2016.

[23] P. Qian, Y. Guo, N. Li, and D. Fang, "Compressive sensing based multiple source localization in the presence of sensor position uncertainty and nonuniform noise," *IEEE Access*, vol. 6, pp. 36571–36583, 2018.

[24] J. Chen, M. Zhu, and F. Tufvesson, "SLAM using LTE multipath component delays," in *Proceedings of IEEE Vehicular Technology Conference*, pp. 1–5, 2020.

[25] D. Rodriguez, J. Apolinario, and W. Martins, "Robust passive coherent location via nonlinearly constrained least squares," in *Proceedings of IEEE Latin America Symposium on Circuits and System*, pp. 1–4, 2021.

[26] Z. Mao, H. Su, B. He, and X. Jing, "Moving source localization in passive sensor network with location uncertainty," *IEEE Signal Processing Letters*, vol. 28, pp. 823–827, 2021.

[27] G. Yang, Y. Yan, H. Wang, and X. Shen, "Improved robust TOA-based source localization with individual constraint of sensor location uncertainty," *Signal Processing*, vol. 196, pp. 1–13, 2022.

[28] Y. Zhang and K. Ho, "Localization of transmitters and scatterers by single receiver," *IEEE Transactions on Signal Processing*, vol. 71, pp. 2267–2282, 2023.

[29] F. Li, T. Jin, H. Qin, and J. Qu, "Asynchronous terrestrial signal of opportunity-based self-localization with source location uncertainty: Methods and analysis," *IEEE Transactions on Aerospace and Electronic Systems*, no. 1–11, p. accepted, 2024.

[30] A. Sel, S. Hayek, and Z. Kassas, "Robust position estimation using range measurements from transmitters with inaccurate positions," in *Proceedings of International Conference on Information Fusion*, pp. 1–6, 2024.

[31] Y. Zhao, X. Li, Y. Wang, and C. Xu, "Biased constrained hybrid kalman filter for range-based indoor localization," *IEEE Sensors Journal*, vol. 18, no. 4, pp. 1647–1655, 2018.

[32] S. Tomic and M. Beko, "A min-max optimization-based approach for secure localization in wireless networks," *IEEE Transactions on Vehicular Technology*, vol. 73, pp. 4151–4161, October 2024.

[33] Z. Kassas, J. Khalife, A. Abdallah, and C. Lee, "I am not afraid of the GPS jammer: resilient navigation via signals of opportunity in GPS-denied environments," *IEEE Aerospace and Electronic Systems Magazine*, vol. 37, pp. 4–19, July 2022.

[34] Z. Kassas and A. Abdallah, "No GPS no problem: Exploiting cellular OFDM-based signals for accurate navigation," *IEEE Transactions on Aerospace and Electronic Systems*, vol. 59, pp. 9792–9798, December 2023.